A new concept for estimating the influence of vegetation on throughfall kinetic energy using aerial laser scanning

Johannes Antenor Senn,[1,2]* iD **Fabian Ewald Fassnacht,[1]** iD **Jana Eichel,[1,3]** iD **Steffen Seitz[4]** iD **and Sebastian Schmidtlein[1]**
[1] Institute for Geography and Geoecology, Karlsruhe Institute of Technology, Karlsruhe, Germany
[2] School of Engineering, Newcastle University, Newcastle upon Tyne, UK
[3] Department of Physical Geography, Utrecht University, Princetonlaan 8a, 3584 CB Utrecht, The Netherlands
[4] Department of Geosciences, University of Tübingen, Tübingen, Germany

*Correspondence to: Johannes Antenor Senn, School of Engineering, Cassie Building, Newcastle Upon Tyne, NE1 7RU, UK. E-mail: j.senn@newcastle.ac.uk

ESPL
Earth Surface Processes and Landforms

ABSTRACT: Soil loss caused by erosion has enormous economic and social impacts. Splash effects of rainfall are an important driver of erosion processes; however, effects of vegetation on splash erosion are still not fully understood. Splash erosion processes under vegetation are investigated by means of throughfall kinetic energy (TKE). Previous studies on TKE utilized a heterogeneous set of plant and canopy parameters to assess vegetation's influence on erosion by rain splash but remained on individual plant- or plot-levels. In the present study we developed a method for the area-wide estimation of the influence of vegetation on TKE using remote sensing methods. In a literature review we identified key vegetation variables influencing splash erosion and developed a conceptual model to describe the interaction of vegetation and raindrops. Our model considers both amplifying and protecting effect of vegetation layers according to their height above the ground and aggregates them into a new indicator: the Vegetation Splash Factor (VSF). It is based on the proportional contribution of drips per layer, which can be calculated via the vegetation cover profile from airborne LiDAR datasets. In a case study, we calculated the VSF using a LiDAR dataset for La Campana National Park in central Chile. The studied catchment comprises a heterogeneous mosaic of vegetation layer combinations and types and is hence well suited to test the approach. We calculated a VSF map showing the relation between vegetation structure and its expected influence on TKE. Mean VSF was 1.42, indicating amplifying overall effect of vegetation on TKE that was present in 81% of the area. Values below 1 indicating a protective effect were calculated for 19% of the area. For future work, we recommend refining the weighting factor by calibration to local conditions using field-reference data and comparing the VSF with TKE field measurements. © 2020 The Authors. Earth Surface Processes and Landforms published by John Wiley & Sons Ltd

KEYWORDS: splash erosion; throughfall kinetic energy; remote sensing; LiDAR; Vegetation Splash Factor

Introduction

Soil erosion is a natural process that is sensitive to changes of land use and climate. In areas with intensive agricultural cultivation enormous economic and social consequences can arise from disturbed soil erosion dynamics (Morgan, 2005). Increased soil erosion can result in nutrient leaching, declining crop yields, reduced biodiversity or decreasing soil filtering functions with potential effects on water resources (Giambelluca et al., 2009). Furthermore, soil erosion can reduce the water retention capacity and hence increase flood risk (Morgan, 2005; Hiraoka and Onda, 2012). In its undisturbed condition, soil is typically resistant against transport processes. Consequently, the initial process of soil erosion is disturbance, or more precisely the disintegration of soil aggregates by bioturbation, wetting–drying processes, freeze–thaw cycles or splash effects caused by raindrops (Arnalds, 2000;

Geißler, 2011). This results in loose soil particles, which are more prone to transport processes driven by water or wind (Panagos et al., 2015). Splash erosion is disintegrating soil aggregates by impacting drops of water and initiating their short-range transport (Morgan, 2005; Blanco-Canqui and Lal, 2008). In the literature, splash erosion has been described as the most important detaching agent (Shinohara et al., 2018). The intensity of splash erosion at a particular site mostly depends on the erodibility of the local soil surface and the kinetic energy of the impacting drop. Soil erodibility varies with grain size, chemistry of the soil matrix and the content of organic matter which all influence soil shear strength. Rock fragments can act as a protective cover against drop impacts (Panagos et al., 2014). The kinetic energy of an impacting drop depends on its size and falling height which in turn are determined by the precipitation type and the additional effect of vegetation. Natural precipitation is highly variable and

strongly modified by the presence of vegetation (Levia et al., 2017). This influence of vegetation layers on splash erosion is investigated as 'throughfall kinetic energy' (TKE) compared to 'freefall kinetic energy' (FKE).

Vegetation generally plays an important yet not fully understood role in controlling soil erosion as it can both aggravate and diminish disintegration processes. In erosion models the influence of vegetation is simplified, e.g. as density-dependent protective parameter or as a set of predefined crop classes in empirical models such as the universal soil loss equation, USLE (Wischmeier et al., 1978). In fact, vegetation canopies closely above the soil surface reduce surface run off, stabilize soil and protect the surface from direct drop impact. These processes have been well investigated (Ferro and Minacapilli, 1995; Wang et al., 2013). However, the influence of higher vegetation layers (e.g. formed by shrubs and trees) have received less attention (Goebes et al., 2015a) but are likely to play a crucial role in splash erosion processes. In any case, those processes are not reflected in detail within erosion models.

Rainfall erosivity is controlled by the duration, magnitude and intensity of a rainfall event (Panagos et al., 2015). The drop size distribution (DSD) provides information on the intensity of rainfall, as the potential drop velocity and hence kinetic energy increases with drop size (Van Dijk et al., 2002). The falling height required to reach terminal velocity also increases with drop size: The largest drops must fall at least 12 m to reach terminal velocity, whereas smaller drops are more likely to reach terminal velocity (Wang and Pruppacher, 1977).

Interception processes caused by vegetation do not only influence the DSD, but also the temporal, spatial and proportional distribution of raindrops reaching the ground. Depending on its path through the vegetation, precipitation is grouped into three components when passing through vegetation: Interception, stemflow and throughfall. Water retention on the plant surfaces is called canopy interception and its magnitude is determined by canopy storage capacity. In the course of rainfall events the canopy saturation by incremental wetting of stems and leaves causes an increase in drip formation. This throughfall lag results in a successive shift in DSD with an increasing proportion of larger drops from leaf drips (Nanko et al., 2008b). In arid climates evaporation rates must be additionally considered (Van Dijk and Bruijnzeel, 2001). The second rainfall component that is not contributing to throughfall is the stemflow. It is generated by water running along the downside of upward oriented branches towards the stem (Herwitz, 1987; Park and Cameron, 2008; Levia and Germer, 2015) and then along the stem to the ground. The DSD of throughfall is determined by its path through the canopy and thus crucial for the understanding of TKE. Throughfall consists of three drop components: free throughfall, splash droplets and canopy drips (Nanko et al., 2006). Raindrops passing through the canopy without striking the vegetation are called free throughfall. Their DSD equals open rainfall. Splash droplets are formed by the impact of drops on surfaces and have diameters of < 1.5 mm (Levia et al., 2017, 2019). The number of droplets increases with windspeed and rainfall intensity because the number of droplets produced per impact increases with kinetic energy (Herwitz, 1985; Murakami, 2006; Nanko et al., 2006). Canopy drips have the largest diameters among the throughfall components and can thus reach the highest kinetic energy.

Throughfall generation can be estimated with several well-established models: The models of Gash (1979) and Rutter et al. (1971) have both been continuously improved and been applied area-wide using remote sensing data (de Jong and Jetten, 2007). In contrast, there are no established methods available for the area-wide estimation of DSD or TKE. Previous studies agree that the rainfall intensity, independent from

vegetation, is the most influential parameter driving splash erosion (Blanco-Canqui and Lal, 2008; Liu et al., 2018). Nevertheless, vegetation is assumed to have a significant impact and some recent studies investigated vegetation effects in relation to land-use and vegetation type: Lacombe et al. (2018) found high TKE in land-cover types with sparse but high vegetation while they found notable reduced TKE in land-cover types with a low and dense vegetation layer. Similar findings were described by Liu et al. (2018) in plantation forests without pronounced understory and under maize canopy by Liu et al. (2016). This coincides with the findings of earlier studies (Seitz et al., 2015; Goebes et al., 2015a) emphasizing the protective effect of understory and litter cover against impacting rain splash. However, these studies are based on occurrences of broad growth form classes (herbs/crops, shrubs, trees) and their arrangements which we consider imprecise for describing the influence of vegetation on TKE. For example, in some cases a differentiation between a bush and a tree of the same height may not be meaningful as the decisive property of both plants is likely to be the crown base height which does not necessarily differ between the two plants. Hence, we think that a continuous structure-based approach which focuses on the continuous arrangement of plant elements in the three-dimensional (3D) space can be a more effective approach than a distinction based on plant types.

Another important aspect which has rarely been addressed is the data-driven estimation and mapping of TKE across larger regions. The latter is an important requirement for environmental protection and risk assessment related to erosion effects as such assessment are typically conducted on a regional level. There have been some earlier studies, including for example Zhongming et al. (2010) who applied remote sensing methods to assess general erosion risk using passive multispectral satellite data. These studies estimated TKE or erosion risk using indirect relations based on vegetation cover and type but did not account for variability in TKE created by the arrangement of plant elements in 3D space, which is known to be a major determinant of TKE.

A larger potential to derive such 3D information on vegetation structure has been identified for increasingly available airborne and terrestrial laser scanning technologies (Hosoi et al., 2010) also known as Light Detection and Ranging (LiDAR). Such systems have been proven to efficiently determine vegetation top height (Popescu et al., 2002), crown base height (Popescu and Zhao, 2008), as well as the presence of understory vegetation layers (Korpela et al., 2012). It is hence likely that LiDAR data offers interesting opportunities for implementing a spatially continuous approach to estimate the effects of vegetation on TKE. However, such an approach is yet to be developed.

The objectives of the present study are hence (i) to identify the structural vegetation parameters controlling TKE from a literature survey, (ii) to formulate a conceptual model of the interaction between FKE and structural vegetation parameters and (iii) to develop a method for the area-wide representation of this interaction via a single measure that can be derived using LiDAR data. The latter methods will be implemented for a spatially continuous LiDAR dataset available for a catchment with heterogeneous vegetation structures in central Chile.

Methods

Development of the Vegetation Splash Factor

To identify the vegetation parameters controlling TKE, a literature review was conducted on throughfall generation and TKE

which are closely linked. In previous TKE studies, many different vegetation parameters have been investigated on plot, individual plant or species level depending on the objectives of the study. To evaluate the relevance of a range of vegetation parameters regarding our objectives, they are assessed by two criteria: (i) predictive value for TKE and (ii) independence from other parameters. Furthermore, we assessed whether the parameter reflects the vertical or the horizontal vegetation structure, or both (3D). We also determined whether the parameter can be measured or estimated at large-scale and area-wide by use of remote sensing techniques. In our assessment, we furthermore tried to focus on vegetation parameters that we assume to have a direct (physical) influence on raindrops and hence TKE while we avoid vegetation parameters that may indirectly correlate with TKE. For example, tree age is likely to correlate with tree height, but tree height is the factor that physically influences TKE. In the following, the vegetation parameters are presented along an increasing object scale: we start with parameters assessed on single leaf-level, continue with parameters on a branch-level and then review parameters related to vertical, horizontal and 3D canopy-structure (Table I).

Leaf and branch characteristics

Leaf properties were for example investigated by Goebes et al. (2016) who identified the leaf area as having the highest influence on TKE from a range of vegetation parameters. Leaf area represents the surface available for raindrop gathering and confluence and is therefore determining the size of leaf drips. Several other studies conducted in the field (Calder, 2001; Nanko et al., 2006) and under experimental conditions (Herwitz, 1987) support the high relevance of leaf areas for estimating TKE. In addition, leaf shape (Hall and Calder, 1993; Goebes et al., 2015a), leaf surface (Nanko et al., 2013), water repellency (Rosado and Holder, 2013) and leaf angle (Park and Cameron, 2008; Nanko et al., 2013) were found to have strong influence on TKE. However, these parameters are also all highly intercorrelated (Foot and Morgan, 2005). Goebes et al. (2015a) measured the second highest variation in TKE between deciduous and evergreen species. However, leaf habit relates to a variety of different traits: Evergreen species tend to have smaller leaf areas, larger crown heights and thus higher falling heights and a higher Leaf Area Index (LAI). Additionally, the seasonal transformation of phenology causes significant differences in the vegetation structure (Nanko et al., 2016). For this reason, foliation cannot be investigated independently from other seasonal variables like temperature and solar inclination which in turn are affecting evaporation, viscosity and surface tension of water (Levia and Herwitz, 2000).

Focusing on branches and other wooden structures, Crockford and Richardson (2000) found that branch angles have a large impact on the throughfall-stemflow distribution. Besides branch angles Levia et al. (2015) identified branch count and dry woody biomass as most important parameters influencing stemflow yield. Other studies found that the bark roughness is strongly correlated with the spatial DSD (Herwitz, 1987; Park and Cameron, 2008). In aforementioned studies, leaf and branch properties were amongst the most influential parameters determining TKE. They are, however, often intercorrelated and their importance is hard to isolate. Furthermore, leaf and branch parameters are mostly suitable for measurements on plot and plant level but can hardly be obtained for area-wide assessments.

Vegetation parameters related to vertical structure

The vertical vegetation structure affects the potential falling heights of raindrops and thereby TKE. The most dominant expression of vertical vegetation structure is the plant height,

Table I. Vegetation parameters influencing throughfall kinetic energy (TKE)

	Leaf and branch characteristics					Vertical structure				Horizontal structure		Based on process-understanding			
	Leaf area	Leaf shape/ angle/ surface	Leaf habit/ seasonality	Branch angles	Bark roughness	Tree height	Crown base height	Number of branches	Canopy thickness	Leaf Area Index (LAI)	Vegetation cover	Two-layer model	Stratified vegetation cover index	Alternative LAI	Leaf area density (LAD)
Predictive value	X	X	X	X	X	X	X		X	X	X				
Independence	X			X		X				X	X				
Area-wide		X	X	X		X	X			X	X	X	X	X	X
Vertical			X		X	X	X	X	X	X		X	X	X	X
Horizontal	X	X								X	X		X	X	X

which determines the potential maximum falling height and thus, the maximum kinetic energy of drips. Accordingly, several studies found a strong correlation between plant height and TKE (Foot and Morgan, 2005; Geißler et al., 2013; Goebes et al., 2015a). The crown base height (CBH) can be seen as 'the last barrier' of the canopy (Goebes et al., 2015a) determining the lowest falling height of drips. Although, CBH is found to be rather influential on TKE (Nanko et al., 2008b; Goebes et al., 2016) it does not represent the whole vegetation: The presence of shrubs and other vegetation below the crown lead to re-interception.

Further parameters reflecting vertical distribution in previous studies are the number of branches (Herwitz, 1987; Goebes et al., 2015b) and the canopy thickness (Nanko et al., 2008b). These parameters do not give any indication of potential falling heights. Neither do they reflect the vertical distribution of vegetation density which could provide information on drip origins. We hence assume that number of branches and canopy thickness are only significant for TKE through their intercorrelation with other parameters.

Finally, understory elements and particularly dense and low canopy layers are suspected to have a notable influence on TKE as they can form a protective layer intercepting canopy drips with high kinetic energy (Foot and Morgan, 2005). Such low vegetation layers (mostly grasses, herbs and small shrubs) and litter cover might be more influential on soil loss than higher canopy layers (Zhongming et al., 2010) and should certainly be included when modelling TKE under the influence of vegetation. Assessment of such low canopy layers with remote sensing methods is challenging and under some conditions even impossible. Particularly the presence or absence of litter under canopy will in most cases not be possible, while the presence of smaller shrubs and even herbal layers may be detected with high resolution or full waveform LiDAR data (Hollaus et al., 2010). The presence of litter under the canopy may partly be predictable based on the species occurring in the canopy as the degradability of leaves varies amongst species. Remote sensing-based mapping of dominant tree and shrub species has been widely documented in the literature (Fassnacht et al., 2016; Kattenborn et al., 2019a).

Vegetation parameters related to horizontal structure

Cover-related variables contain information on the horizontal distribution of the vegetation that can be utilized to approximate the storage capacity of vegetation surfaces but also free throughfall through gaps. One important horizontal variable is LAI, which is defined as the total leaf surface per unit of ground surface. The surface area determines storage capacity and therefore the magnitude of throughfall lag, the retention of water on the vegetation surface. It also affects the probability of re-interception by lower vegetation layers, which determines the proportion of droplets. Furthermore, LAI can be related to the canopy cover and thus to canopy gaps that allow free throughfall (Gonsamo et al., 2013). However, for the relation of LAI and TKE inconsistent findings are described in previous studies. For example, Nanko et al. (2008a) and Geißler et al. (2013) found a negative influence of LAI on TKE below trees larger than 15 m. Goebes et al. (2016) in contrast, found a positive correlation of LAI and TKE in an early-successional forest plantation. These differences might result from differences in the vertical distribution of the leaf area, especially due to varying vegetation heights.

Variables related to horizontal structure have been successfully approximated from various remote sensing data types and across several land-cover types. Studies applied both passive spectral data (e.g. Wood et al., 2012) and active LiDAR data [e.g. Dandois and Ellis, 2010 or Lefsky et al., 2002].

### Approaches based on process-understanding

Besides the discussed individual plant parameters, some integrated approaches have been suggested to describe vegetation effects in the context of TKE and erosion modelling. For example, the Stratified Vegetation Cover Index (SVCI) suggested by Zhongming et al. (2010) features four classes of vegetation layers: trees, shrub, grass and litter. Erosion intensities are then approximated by summing up the densities of the four layers and an empirical weighting factor. Zhongming et al. (2010) developed this concept based on reference vegetation mapped on field plots and the erosion measured below. Subsequently, Landsat data were used across larger areas to identify vegetation similar to the reference types and to assign the measured erosion rates to them.

The alternative Leaf Area Index (aLAI) proposed by Foot and Morgan (2005) is similar to SVCI, but here the layers are separated by height instead of plant type. In the aLAI concept, TKE is modelled as the sum of vegetation layers weighted depending on their height. Although this structure-based approach allows a high degree of comparability between studies, the index could not be successfully related to TKE. We assume that the approach neglects the protective effect of lower layers, which is particularly important as the investigated vegetation did not exceed 60 cm.

Finally, we identified another relevant variable: The gap fraction profile and its counterpart the vegetation cover profile. The vegetation cover is defined as the proportion of horizontal vegetated area occupied by the vertical projection of canopy elements (Gonsamo et al., 2013). It can be determined for a series of vertical vegetation layers as vegetation cover and gap fraction profile. The vegetation cover profile can be calculated in a regular horizontal grid spanning across the area of interest. The resulting 3D grid is called voxel space. It reflects both vertical and horizontal distribution of vegetation in space and can be calculated from small footprint airborne LiDAR as shown in some earlier studies (e.g. Bouvier et al., 2015).

Implications – setting up a conceptual vegetation splash model

Based on the earlier review, we assume that both, the horizontal and the vertical distribution of vegetation must be considered to successfully predict TKE. Additionally, some highly influential leaf and branching parameters were identified. Further complexity is added by the seasonal variation of some of the identified parameters. One option to successfully predict TKE may be the integration of all these important vegetation parameters into a complex model. However, it is likely that such a model would be difficult to calibrate and parameterize as reliable measurements of many (partly intercorrelated) vegetation parameters would be necessary. Furthermore, an accurate large-scale and area-wide estimation of these parameters seems very challenging. Here, we hence suggest a simpler conceptual model that is solely based on the gap fraction profile. In this context we interpret the gap fraction as the probability of throughfall within a layer assuming a homogeneous spatial distribution of gaps over the base area for simplification. The literature review led us to the hypothesis that the influence of vegetation on TKE varies with the vegetation height and arrangement: Lower vegetation acts as protective layer reducing TKE, whereas higher vegetation amplifies TKE through increased falling heights of (large) canopy drips and splash droplets. Figures 1A–1D schematically illustrates the assumed interaction of the opposing effects of vegetation layers on TKE. In the reference state (Figure 1A) the TKE equals FKE.
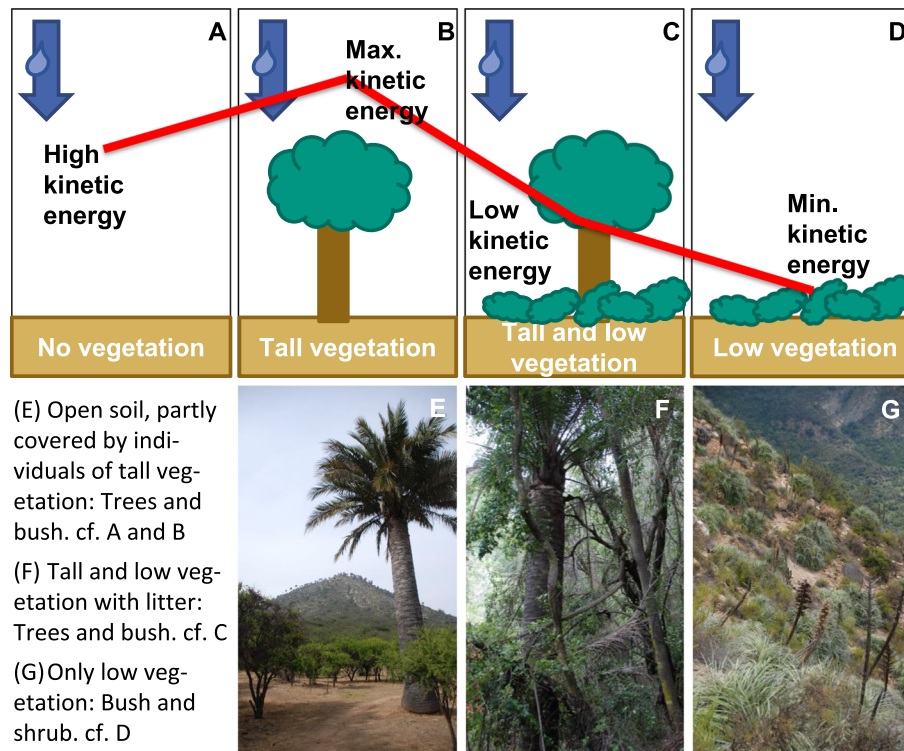
Figure 1. Schematic representation of layer-based approach of vegetation impact on throughfall kinetic energy (TKE) (A–D) and examples for corresponding vertical vegetation structures (E–G) in La Campana National Park. [Colour figure can be viewed at wileyonlinelibrary.com]

Increased or decreased TKE is expected in the presence of exclusively tall or low vegetation (Figures 1B and 1D). Whereas the effects of tall vegetation and protective low vegetation layer outbalance each other when combined (Figure 1C). This assumption is supported by the findings of Lacombe et al. (2018) where the only scenario with TKE lower than FKE was found for low vegetation.

Based on these findings we propose a new measure for the influence of vegetation on TKE: the Vegetation Splash Factor (VSF). To understand where drops originate from, it is easiest to imagine looking at the vegetation from the ground: Free throughfall precipitates onto areas where sky is visible and drips fall from the lowest visible vegetation layer. The area proportions per layer from which drips can fall to the ground without being intercepted can be transferred into a vertical profile of the drip contribution (DC).

Here, we derive the DC from the vegetation cover, because DC cannot be measured directly. We assume the probability of throughfall and interception in a vegetation layer depends on the ratio of vegetation cover and gap fractions. To estimate DC we hence divide the vegetation into a series of vertical layers and measure their gap fractions to estimate the probability for leaf drips to reach the ground without re-interception in lower layers. The model is illustrated in Figure 2 by means of a simplified vegetation structure (background): The proportions of vegetation cover and gap fraction (Figure 2a) are visualized in a bar graph and reflect the canopy and understory. The shading indicates the proportion of precipitation reaching the ground without being intercepted below. To account for free throughfall we introduced an artificial layer with 100% cover above the vegetation representing open rainfall.

To calculate the VSF, we follow two steps. In the first step we determine the drip contribution in the vegetation profile. The second step is to assign a weighting factor to include the influence of the vegetation elements on kinetic energy. We know that the kinetic energy is defined as the work required to accelerate a drop of a given mass to a stated velocity, which is determined by both, falling height and drop diameter. The largest drops reach terminal velocity after 12 m (Gunn and Kinzer, 1949). The falling height required to reach the same kinetic energy of a drop in open rainfall decreases with drop diameter (van Dijk et al., 2002; Goebes et al., 2014). Below a certain falling height, the kinetic energy of drips becomes smaller compared to FKE. In this case we assume that vegetation reduces the kinetic energy of rainfall. If we assume that drips under one specific species have similar DSD we narrow the determining factors for TKE down to the falling height. Thus, the weighting factor is mainly based on the kinetic energy of drips according to their falling height. The height where the TKE of canopy drips exceeds FKE and hence the weighting factor (WF) = 1 varies with vegetation types. For simplification, we estimated the weighting factor from the literature by comparing the kinetic energy of many different drip and raindrop sizes falling from different heights (cf. Wainwright et al., 1999; van Dijk et al., 2002; Goebes et al., 2014). We assume that 1 m is a good estimation for the average DSD to reach TKE = FKE. Analogously we assume WF = 3 as upper limit for the amplifying effect (Lacombe et al., 2018; Liu et al., 2018). The weighting factor curve shown in Figure 2c is a first suggestion based on the assumed relation between TKE and vegetation height. Finally, we calculated the VSF as the sum of the weighted DC profile. The VSF indicates the effect of vegetation on TKE relative to FKE and assumes values greater than 1 for amplification and less than 1 for protection. Consequently, the WF is 1 for the open rainfall layer above the vegetation. In order to reproduce the actual relations in a given area, the weighting factors must be calibrated based on field measurements, which were not available in the scope of this study but will be part of an upcoming field campaign. The calibration must include the typical range of rainfall intensities and durations in order to register characteristic DSD and the effect of throughfall lag. Nevertheless, we implemented the VSF for a dataset in a heterogeneous study area in central Chile for a first plausibility check.
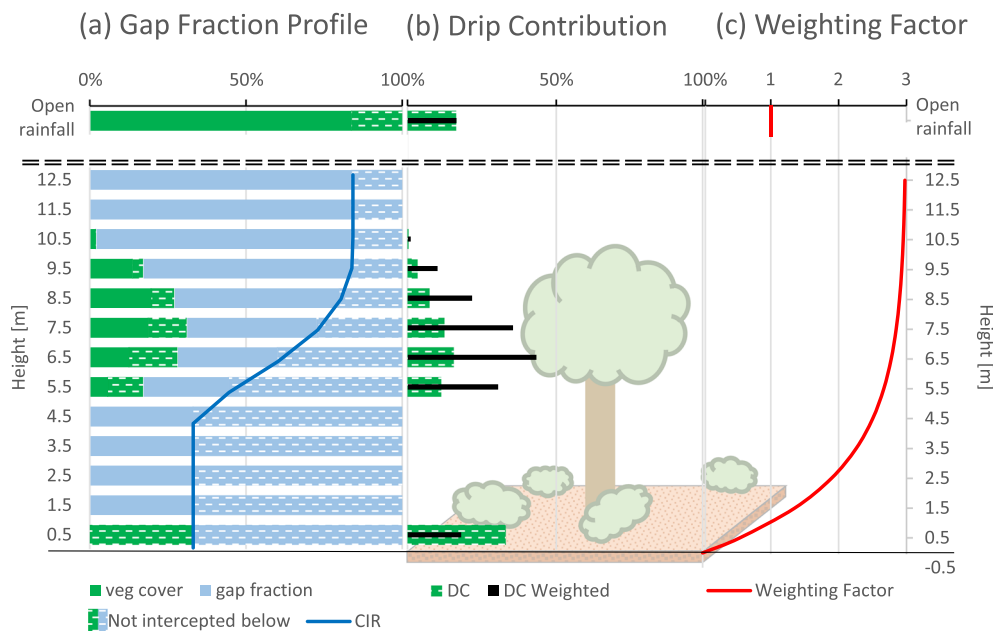
Figure 2. Schematic representation of the conceptual model on an exemplified vegetation profile (background). Note that in the model, as opposed to this figure, vegetation cover and gaps are distributed homogeneously inside the individual layers. (a) Percentage of gap fraction (blue) and vegetation cover (green), dashed areas indicate free throughfall below, the solid share is intercepted in the layers below. The blue line indicates the cumulative interception ratio (CIR). (b) The drip contribution (DC) profile indicates the percentage of drips from a layer falling without interception below. When applying the weighting factor (c) the weighted drip contribution reflects the effect of the layer on TKE. The largest drop only reaches terminal velocity after 12 m falling height (Gunn and Kinzer, 1949). [Colour figure can be viewed at wileyonlinelibrary.com]

Case study

To implement the conceptual model for an area wide application we divided an airborne laser scanning point cloud into a grid of regular cells. Then, we derived the gap fraction and DC profiles for every cell and calculated the VSF as a raster. Finally, we assessed the results for plausibility and consistency (Figure 3).

The experimental site is situated in the La Campana National Park near Ocoa, Valparaiso, central Chile and is part of the EarthShape project [DFG SPP 1803, see Bernhard et al., 2018 and Schmid et al., 2018]. It features a heterogeneous mosaic of vegetation layer combinations on a total area of 49 km², rising from 400 to 2200 m above sea level (a.s.l.). The vegetation structure of the area ranges from open land, low vegetation with bushes and shrubs, mixed low/tall vegetation to tall vegetation mainly dominated by Chilean palms (Figure 1). Airborne LiDAR scans were conducted by Digimapas Chile Aerofotogrammetra Ltda on the 10 and 13 September 2016.

The discrete return LiDAR dataset features a density of three to five points per square metre and covers a total area of 4258 ha. Each point contains values for intensity and number of returns with up to seven returns per pulse.

To calculate the VSF, we first normalized the point cloud by subtracting the heights of a digital terrain model (DTM) from the individual point height using TreesVis (Weinacker et al., 2004). In the next step we used R (R Core Team, 2016) and the lidR package (Roussel and Auty, 2019) to calculate the gap fraction profile. For each voxel in a 5 m × 5 m grid with 1 m layer height we calculated the gap fraction profile as the ratio of returns below and above the voxel with a lower threshold of 0.1 m (Bouvier et al., 2015). All returns below this threshold are considered as ground. Assuming that laser beams behave similar to sunlight the gap fraction profile is equivalent to canopy transmittance according to the Beer–Lambert law (Breda, 2003) and thus reflects the vertical distribution of vegetation (Bouvier et al., 2015). The calculation method is described for a single grid cell. The gap fraction (GF) for a layer i is calculated as:
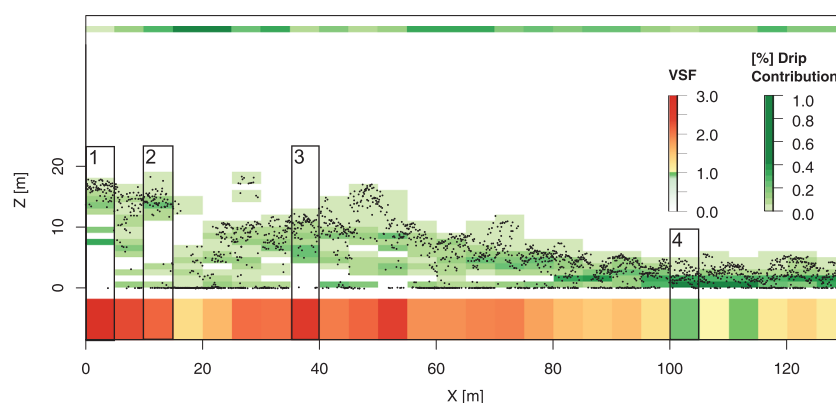

Figure 3. Transect (height against *X* coordinate) of the point cloud underlain by the calculated drip contribution (DC) pro-file raster and the resulting Vegetation Splash Factor (VSF) below. The area covered by the transect is indicated in Figure 4. The boxes indicate where the amplifying (1, 2 and 3) and protective effect (4) can be observed. [Colour figure can be viewed at wileyonlinelibrary.com]

$$GF_i = \frac{N_{[0;z]}}{N_{total} - N_{[0;z+dz]}}$$

with $N_{[0;z]}$ being the number of returns below z, N_{total} the total number of returns, and $N_{[0;z+dz]}$ the number of returns below $z + dz$ (Bouvier et al., 2015). The gap fractions are illustrated as blue bars in Figure 2a.

The selected voxel size is a trade-off between accuracy (points per voxel) and resolution (voxel footprint): We chose a comparably large grid size according to the relatively sparse point cloud density of three to five points per square metre of the available LiDAR dataset.

The vegetation cover (VC) profile is calculated as (Gonsamo et al., 2013):

$$VC_i = 1 - GF_i$$

and illustrated with green bars in Figure 2a. Next, we calculated the cumulative interception ratio (CIR), the percentage of interception in and below every layer (blue line in Figure 2 a). For the lowest layer (0.1–1.1 m in our vertical resolution) CIR equals the vegetation cover. In the subsequent layers above it is calculated as:

$$CIR_i = VC_i + GF_i * CIR_{i-1}$$

An increase in CIR between two layers indicates that drips from this layer reach open ground. Finally, the difference between the CIR of each layer and its predecessor is the DC value. It is calculated as:

$$DC_i = CIR_i - CIR_{i-1}$$

In Figure 2a the shaded green areas illustrate the DC as part of the vegetation cover and in Figure 2b as isolated profile. By definition the sum of the drip contribution profile is 1 as it represents proportions of the unit of ground that is either reached by drips or free throughfall.

Then, we calculated the weighted DC profile (see Figure 2b, black lines) by applying the height dependent weighting factor (see Figure 2c) to every voxel. The weighting factor ensures that

the weighted drip contribution of lower layers reduce TKE whereas higher layers amplify it and is ideally calibrated with TKE measurements. Based on our estimation it is calculated as:

$$WF = 3 - 3 * e^{-0.4*h}$$

where h is the voxel elevation. The equation applies for vegetation bodies while the WF for above the vegetation is fixed to 1. Finally, we summed up the weighted DC values over each grid cell to yield the VSF.

$$VSF = \sum_{i=h_{min}}^{h_{max}} DC_i * WF_i$$

With this approach, we calculated a VSF map of the entire study area and extracted subsets to visually interpret and discuss the results on the basis of an unmanned aerial vehicle (UAV) orthophoto (Figure 4). Additionally, a vertical profile through the point cloud was extracted along a transect and the calculated DC profile was plotted to assess the plausibility of the implementation of the conceptual model (Figure 3). The location of the transect is marked in Figure 4.

Results

In the investigated area we calculated a mean VSF of 1.42 (median: 1.32). Values below 1 were calculated for 19% of the area, while the other 81% show values above 1 (cf. Table II). The vertical distribution of aerial LiDAR returns and the calculated DC for an exemplary transect are illustrated in Figure 3. In addition, Figure 3 features the calculated VSF values as a stripe below the profile. The highest VSF values occur in grid cells with almost no ground returns (cf. boxes 1 and 3). Whereas, grid cells with large numbers of returns in the lowest layers show more variability in the resulting VSF values depending on the height and DC of the overlying voxels (cf. boxes 2 and 4). The higher canopy layers in box 2 coincide with a higher VSF value. In box 4 however, the falling heights are lower and thus the calculated VSF. In grid cells with dense canopies
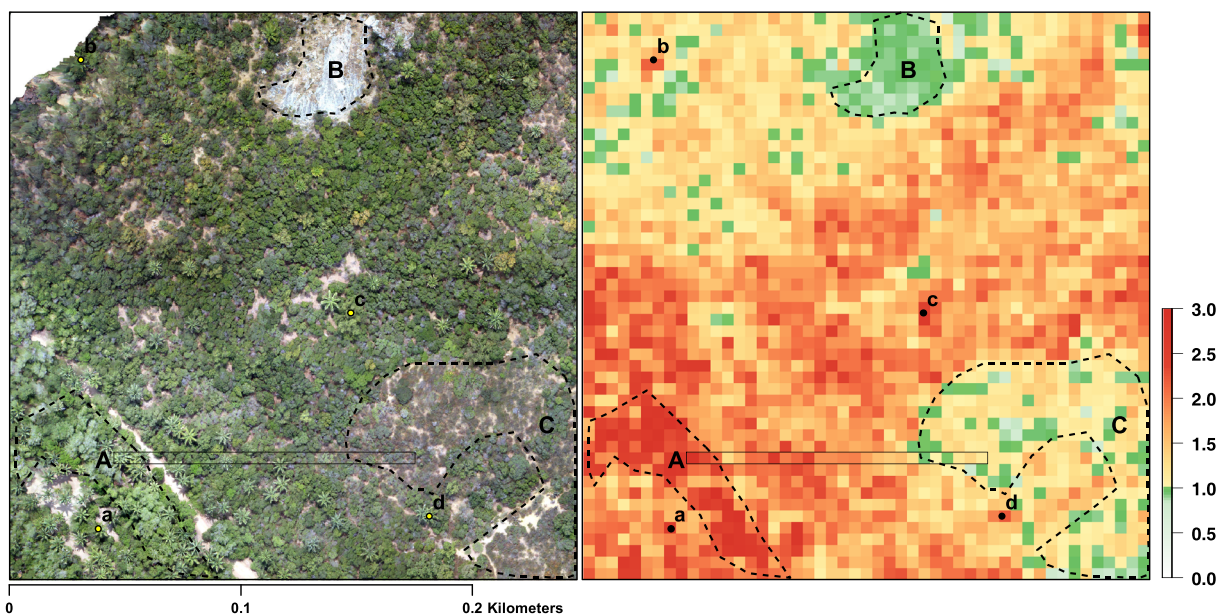

Figure 4.   A subset of the calculated Vegetation Splash Factor (VSF) map with an unmanned aerial vehicle (UAV) ortophoto as reference. The black box (solid line) indicates the location of the transect of Figure 3 for context. Three polygons (dashed lines) and four points indicate areas with characteristic vegetation structures for isolated analysis, see Table II for key statistics. [Colour figure can be viewed at wileyonlinelibrary.com]

Table II. Key statistics for the three polygons (Figure 4) and the whole tile. Heights from the normalized digital surface model, Vegetation Splash Factor (VSF) and vegetation cover of the lowest layer (0.1–1.1 m)

Polygon	Vegetation height (m)			VSF			Vegetation cover fraction 0.1–1.1 m		
	Minimum	Maximum	Mean	Minimum	Maximum	Mean	Minimum	Maximum	Mean
A	0.00	24.20	12.95	1.52	2.88	2.33	0.00	0.40	0.04
B	0.00	4.45	0.19	0.84	1.04	0.92	0.04	0.43	0.21
C	0.00	10.90	2.32	0.71	1.66	1.13	0.00	0.80	0.34
Total	0.00	24.20	4.53	0.64	2.91	1.42	0.00	0.90	0.24

an absence of returns from ground and understory layers can be observed, as some ground voxels do not contain any points.

The VSF map can be related to recognizable structures in the aerial photograph (Figure 4): The lowest VSF values are present in the barely vegetation covered area (21% cover in lowest layer) (polygon B) with a mean VSF of 0.9 (cf. Table II). The surfaces appearing white and grey in the aerial image are mostly bare rock whereas the darker areas in brown and beige show soil and vegetation cover. The average vegetation height in this area is below 20 cm and the VSF values range between 0.8 and 1. Polygon C is characterized predominately by low and intermediate vegetation heights (mean: 2.3 m) with few open areas and patches of higher vegetation up to 10 m. The mean vegetation cover of the lowest layer is 34% and the resulting VSF values range from 0.7 to 1.7 with a mean of 1.1 and are visibly related to the vegetation heights. Consequently, in the valley bottom (polygon A) where water availability allows plant to grow taller (13 m average) we yielded the highest VSF values with a mean of 2.3. The average vegetation cover in the lowest layer is only 4% (cf. Figure 1E photograph from this area). The different vegetation structures in the polygons A and C can be recognized in the vegetation profile (Figure 3) that overlaps the polygons. Further, isolated occurrences of high VSF values can be found scattered over the whole area (cf. points a, b, c, d, Figure 4). These areas often coincide with the large (palm) tree crowns recognizable in the aerial image.

A trail running from southeast to northwest can be recognized in the aerial map parallel to polygon A showing slightly lower VSF values compared to the surrounding high vegetation. However, due to the low spatial resolution a sufficient spatial separation between grid cells with open soil and vegetation is probably not given.

Discussion

Conceptual model and derived Vegetation Splash Factor

Previous work on TKE and vegetation has targeted the understanding of their interaction and thus investigated large numbers of vegetation parameters to quantify their influence on TKE. Our approach, in contrast, focuses on developing a method for the efficient spatially continuous estimation of TKE with as few parameters as necessary. Based on a literature review we identified the main driving vegetation parameters to set up our conceptual model: We suggest that various vertical (e.g. tree height, CBH or canopy thickness) and horizontal parameters (e.g. LAI or canopy cover) can be simplified into a single voxel wise parameter: The vegetation cover profile. This parameter can be derived from aerial LiDAR datasets and is thus more efficient to cover large areas than the parameters used in earlier studies which are typically restricted to small vegetation plots.

The current version of the VSF omits several parameters that the literature review indicates to be influential but are not related to the vertical nor the horizontal distribution of vegetation: The leaf area and branch angles for example have strong impact on the spatial distribution of throughfall and DSD (Herwitz, 1987; Goebes et al., 2016). Further, the temporal variability of TKE (during a rainfall event) is strongly correlated to the water storage capacity and thus LAI (Nanko et al., 2008b). On a larger (e.g. annual) scale the storage capacity varies with foliation (Nanko et al., 2016; Levia et al., 2017). This could be taken into account by considering LiDAR datasets from different seasons.

In a first attempt (not presented here), we calculated the VSF based on the vertical distribution of one-sided leaf area per unit ground surface area, the leaf area density. Although it represents the vertical distribution of biomass (surface area) and thus storage capacity better than the vegetation cover profile, the leaf area density does not reflect the potentials of throughfall and interception. In addition, the leaf area density is an absolute value and is thus limited in its comparability. In the model this led to an overemphasis of dense upper vegetation layers causing high VSF values, which were not outbalanced by the lower layers. This means that the reduction of falling height through re-interception on lower vegetation layers was not considered. For the representation of throughfall probability, the vegetation cover is the more appropriate measure as it is a relative value. By building the model based on the DC, our approach also goes one step further: Only the drops that reach open ground are taken into account in the calculation of the VSF. Therefore, a full vegetation cover in the first layer above the ground cancels out the effect of all layers above.

The height dependent weighting factor is based on the assumption that drops are intercepted on vegetation surfaces. However, drips are more likely to form droplets on impact, while free throughfall drops with smaller diameters tend to remain on the plant surface and build drips. Levia et al. (2019) found that the ratio between throughfall, droplets and drips differ significantly between coniferous and broadleaved vegetation which indicates that the additional consideration of species information may be an interesting future extension for the VSF.

Species information is also relevant in terms of other parameters with a direct effect on TKE. For example, DSD and throughfall amount vary during rainfall events, as canopy storage is successively filled before drips are released (Nanko et al., 2008b; Levia et al., 2019). The storage capacity is known to be related to general parameters as total leaf area but also species-specific parameters such as leaf hydrophobicity or hydrophilicity (Holder, 2012, 2013; Rosado and Holder, 2013). These parameters have significant impact on the hydrological response that can be measured on watershed scale (Holder, 2013). At the same time rainfall intensity creates large variations between events, seasons and regions (Carlyle-Moses and Gash, 2011).

The VSF is currently not taking into account plant specific parameters but follows a purely structure-based approach that can, however, be calibrated to local rainfall and vegetation conditions by adapting the weighting function based on empirical TKE measurements, for example using splash cups (Scholten et al., 2011). Based on this site-specific calibration the VSF estimates the relative effect of vegetation on TKE. This simplification of the model is advantageous as it enables large-scale applications.

However, as indicated earlier, to explain the variation that cannot be related to the VSF, additional species-specific parameters could be collected parallel to the calibration with splash cups (Scholten et al., 2011). In an ideal case, these parameters would also be collected using remote sensing approaches to maintain the possibility to estimate the VSF spatially continuous. Some parameters, e.g. the ratio of wood to leaf surfaces could be directly quantified by classification from aerial imagery, whereas other plant specific parameters could be assigned based on species classification from multispectral or RGB UAV data (Kattenborn et al., 2019b).

In summary, we believe that our suggested approach to condense the information contained in the 3D vegetation structure represented in the vegetation cover into a two-dimensional map to reflect the influence of vegetation on TKE holds great potential. It may be extended and refined using additional species-specific information and by calibration to local field conditions using reference measurements.

Application of Vegetation Splash Factor in the case study

In our study area we observed a mean VSF of 1.42 (median: 1.32). The overall effect of vegetation on the kinetic energy of rainfall is hence an amplification. We calculated VSF values below 1 for 19% of the area and above 1 on the other 81%. Accordingly, we expect that, vegetation reduces kinetic energy of rainfall in less than a fifth of the area. The amplifying overall effect of vegetation on TKE is consistent with the observed vegetation structure: Large areas show only sparse vegetation in the understory layers. The open rainfall is intercepted by the canopy and forms large leaf drips that can fall uninterrupted to the ground gathering high velocities and kinetic energy. This effect has been described in the literature for areas with similar vegetation structures. For example, Liu et al. (2018) reported relative values of 1.84 to 2.3 for TKE within plantations compared to open conditions.

The vegetation structures recognizable in the aerial image agreed well with the VSF values in the map according to our initial assumptions (Figure 4). The open soil area visible in polygon B is sparsely covered by vegetation. The corresponding VSF values show little variation and a mean of 0.92. This agrees with the expected neutral or slightly protective effect of the vegetation. The lowest VSF values in these areas were calculated for the areas with visible sparse vegetation cover, whereas the areas with open rock are closer to 1. The mean vegetation height of only 0.19 m implies that a small proportion of the vegetation returns are above the 0.1 m threshold that excludes ground points in the calculation of the gap fraction. However, the vegetation cover of the lowest layer with a mean vegetation cover of 21% is higher than the aerial image suggests. The reason for this might be that on a small scale of tens of centimetres in a rather steep section the point cloud normalization is reaching its limits. The medium high vegetation in polygon C coincides with VSF values around 1 but with a wider range of VSF values than in polygon B. Despite the relatively dense

vegetation cover (mean: 34%) in the lowest layer, the highest VSF values occur under the tallest vegetation. A likely reason for this is that the second and third vegetation layers are already weighted with factors 1.4 and 1.9. For this reason, slightly higher overall VSF values were calculated in this area even though the vegetation cover in the first layer is relatively dense. Whether these values are realistic or not has to be validated using field experiments. Finally, in polygon A the most erosion prone vegetation structure is visible. The combination of tall trees and sparse understory consistently yields high VSF values which matches well the theoretical assumptions.

Despite the sparseness of the LiDAR dataset the overall large ratio of ground returns (as visible in Figure 3) indicates that the point cloud density was sufficient for the calculation of an accurate DTM (Estornell et al., 2011). However, a higher point cloud resolution holds potential to improve several aspects of the presented VSF model: Firstly, a better horizontal and vertical resolution would allow to reduce the applied grid size and hence to identify gaps on a smaller scale, e.g. the trail running parallel to polygon A. Secondly, it would allow a better representation of variations in the vegetation density and thus a finer differentiation between cover percentages. Thirdly, a finer DTM resolution would reduce the vertical deviations induced by point cloud normalization (which does not account for within-pixel terrain inclinations) and thus improve the accuracy of the derived gap fraction profiles, especially near the ground.

The presence of ground returns in most areas of the dataset proves that individual laser pulses could penetrate the vegetation to the ground: All layers were reached by the scanner and thus considered in the model. Consequently, we assume that few or no returns from the intermediate layers indicate the absence of vegetation and hence free-fall areas that generate high TKE. In turn, the absence of ground returns implies that all pulses were absorbed by vegetation and thus no information on the understory structure is provided (Korpela et al., 2012). Considering the large influence of the lowest vegetation layers on the VSF an adequate representation of these layers is crucial. In the current dataset, this was mostly the case. Deficits in penetration depth can be overcome by reducing the footprint size of the LiDAR scanner (Korpela et al., 2012). Especially, when the VSF is calculated for denser vegetation a higher point cloud density would be required.

In future applications, the normalization process could be improved by using a waveform LiDAR dataset to classify, and filter returns according to echo width and amplitude (Hollaus et al., 2010). This would also allow preventing the misclassification of dense vegetation layers as ground returns, as a result of impenetrability for laser beams. In addition, we want to emphasize the importance of (organic) layers directly overlaying the soil surface such as plant litter, biological soil crusts or stones. Further studies have to evaluate if they can be included in our approach and if litter as wells as biological and non-biological crusting can be efficiently retrieved from spectral remote sensing data or modelled using vegetation type maps and environmental parameters.

Within the first metre above-ground, the protective effect of the low vegetation transforms into the amplifying effect of higher layers (Lacombe et al., 2018; Liu et al., 2018). An accurate vertical representation of the lower layers is therefore crucial for the model accuracy but can be limited by the point cloud density: Voxels must contain a certain number of points to sufficiently reflect variations in vegetation density (Béland et al., 2014). For this reason, we applied a vertical resolution of 1 m in our case study: Hence, only the lowest layer of the drip contribution profile was weighted with values below 1. Low vegetation heights as in polygon B would benefit the most

from a finer vertical resolution where the steep increase of protective effect towards the ground is distributed over more layers. In terms of horizontal resolution, the outcomes of the VSF model would benefit from a better representation of small-scale differences in the vegetation density. In particular, because in the model, as opposed to natural vegetation (see Figure 2), vegetation cover and gaps are distributed homogeneously inside the individual layers. Even though the 5 m grid size was sufficient to prove the concept, future applications require horizontal resolutions of at least 1 m. Overall, we recommend using datasets with at least 10 to 15 pulses per square metre for future applications.

In order to investigate the influence of different LiDAR sensor systems, scan geometries and vegetation properties on the model results, we consider the recent developments in the field of simulated LiDAR scans a promising approach for future investigations (Hämmerle et al., 2017).

Implications

The VSF is a strictly structure-based parameter to efficiently assess vegetation's amplifying and protecting influence on TKE for large areas. Previous concepts are either biased by growth form (SVCI, Zhongming et al., 2010) or did not account for the protective properties of low vegetation layers (aLAI, Foot and Morgan, 2005). While plant and plot-based studies often investigate large numbers of parameters, our approach only uses VSF and we assume that it can represent the majority of these parameters. Compared to the multi-factor approaches of previous studies, the VSF is a strong simplification. At the same time, VSF allows a high level of comparability between studies on soil erosion. This is especially valuable, as meta-analysis and comparison between previous studies on TKE is challenging due to the large number of different investigated parameters. VSF could easily be added to future studies on TKE to improve their comparability. It is even possible to complete previous studies with VSF values if a corresponding LiDAR dataset is available.

The TKE is one of the main factors controlling splash erosion and transport of soil particles. Our concept has great potential to improve future studies on soil erosion as it can be used to estimate splash erosivity by applying the VSF on measured FKE. Combined with soil erodibility parameters and data on soil surface covering vegetation, such as biological soil crusts, this could provide the basis to set up an easy-to-apply erosion model. The VSF could furthermore be included in existing soil erosion models to improve the representation of the influence of vegetation on erosivity. The USLE crop factor for example, could be determined based on actual vegetation structure instead of being roughly classified and assigned to values from species-specific look-up-tables (Wischmeier et al., 1978). If multi-temporal datasets are available the representation of seasonal crops, e.g. corn, grain could be enhanced by considering vegetation periods. VSF can be applied to efficiently map large areas and identify areas of risk. The assessment of areas with VSF values above 1 could be a first step for determining areas that require soil conservation strategies.

Conclusions

In the present study we (i) identified the horizontal and vertical distribution of vegetation as the vegetation parameters with the highest influence on TKE. (ii) Based on these vegetation parameters, we developed a conceptual model of the interaction between TKE and vegetation in which vegetation layers provide protective or amplifying effects on the kinetic energy of rainfall depending on their height and cover. This model was transferred (iii) into a method for the area wide representation of this interaction via a single measure, the VSF that can be calculated from airborne LiDAR datasets. The VSF offers an easily applicable, transferable and standardized measure of the vegetation structure for investigating TKE. We successfully calculated the VSF for a study site in the Chilean La Campana National Park.

The VSF is independent from species composition and thus allows comparisons between sites. To further refine the approach, the weighting factor needs to be calibrated under various types of vegetation by measuring the yielded TKE in the field and assigning it to VSF values.

For future applications, point clouds with higher spatial resolutions are mandatory. This will allow decreasing the grid size and more importantly the layer thickness. We believe that the VSF holds great potential for improving current representations of vegetation in existing soil erosion models and for providing high resolution soil risk maps over large areas.

Declaration of Interest Statement

The authors declare no conflict of interest.

Data Availability Statement

The data sets used and analysed during the current study are available from the corresponding author on reasonable request. The code is available at github.com/Senn-J/VSF

References

Arnalds O. 2000. The Icelandic 'rofabard' soil erosion features. *Earth Surface Processes and Landforms* **25**(1): 17–28.

Béland M, Baldocchi DD, Widlowski JL, Fournier RA, Verstraete MM. 2014. On seeing the wood from the leaves and the role of voxel size in determining leaf area distribution of forests with terrestrial LiDAR. *Agricultural and Forest Meteorology* **184**: 82–97.

Bernhard N, Moskwa LM, Schmidt K, Oeser RA, Aburto F, Bader MY, Baumann K, von Blanckenburg F, Boy J, van den Brink L, Brucker E. 2018. Pedogenic and microbial interrelations to regional climate and local topography: new insights from a climate gradient (arid to humid) along the Coastal Cordillera of Chile. *Catena* **170**: 335–355.

Blanco-Canqui H, Lal R. 2008. *Principles of Soil Conservation and Management* (Vol. 167169. Springer: New York.

Bouvier M, Durrieu S, Fournier RA, Renaud JP. 2015. Generalizing predictive models of forest inventory attributes using an area-based approach with airborne LiDAR data. *Remote Sensing of Environment* **156**: 322–334.

Breda NJJ. 2003. Ground-based measurements of leaf area index: a review of methods, instruments and current controversies. *Journal of Experimental Botany* **54**: 2403–2417.

Calder IR. 2001. Canopy processes: Implications for transpiration, interception and splash induced erosion, ultimately for forest management and water resources. *Plant Ecology* **153**: 203–214.

Carlyle-Moses DE, Gash JHC. 2011. Rainfall interception loss by forest canopies. In *Forest Hydrology and Biogeochemistry*, Levia DF, Carlyle-Moses D, Tanaka T (eds). Springer: Dordrecht; 407–423.

Crockford RH, Richardson DP. 2000. Partitioning of rainfall into throughfall, stemflow and interception: effect of forest type, ground cover and climate. *Hydrological Processes* 14: 2903–2920.

Dandois JP, Ellis EC. 2010. Remote sensing of vegetation structure using computer vision. *Remote Sensing* 2(4): 1157–1176.

de Jong SM, Jetten VG. 2007. Estimating spatial patterns of rainfall interception from remotely sensed vegetation indices and spectral mixture analysis. *International Journal of Geographical Information Science* 21: 529–545.

Estornell J, Ruiz LA, Velázquez-Martí B, Hermosilla T. 2011. Analysis of the factors affecting LiDAR DTM accuracy in a steep shrub area. *International Journal of Digital Earth* 4(6): 521–538.

Fassnacht FE, Latifi H, Stereńczak K, Modzelewska A, Lefsky M, Waser LT, Straub C, Ghosh A. 2016. Review of studies on tree species classification from remotely sensed data. *Remote Sensing of Environment* 186: 64–87.

Ferro V, Minacapilli M. 1995. Sediment delivery processes at basin scale. *Hydrological Sciences Journal* 40: 703–717.

Foot K, Morgan RPC. 2005. The role of leaf inclination, leaf orientation and plant canopy architecture in soil particle detachment by raindrops. *Earth Surface Processes and Landforms* 30: 1509–1520.

Gash JHC. 1979. An analytical model of rainfall interception by forests. *Quarterly Journal of the Royal Meteorological Society* 105: 43–55.

Geißler C. 2011. Mechanisms of Soil Erosion Under Forest Vegetation – Throughfall Kinetic Energy as a Function of Forest Succession and Biodiversity in Subtropical Forests in China, PhD Thesis. Eberhard Karls Universität, Tübingen.

Geißler C, Nadrowski K, Kühn P, Baruffol M, Bruelheide H, Schmid B, Scholten T. 2013. Kinetic energy of throughfall in subtropical forests of SE China – effects of tree canopy structure, functional traits, and biodiversity. *PLoS ONE* 8: e49618.

Giambelluca TW, Sutherland RA, Nanko K, Mudd RG. 2009. Effects of Miconia on hydrology: a first approximation. In *Proceedings of the International* Miconia *Conference*, Keanae, Maui, Hawai'i, 4–7 May.

Goebes P, Bruelheide H, Härdtle W, Kröber W, Kühn P, Li Y, Seitz S, von Oheimb G, Scholten T. 2015a. Species-specific effects on throughfall kinetic energy in subtropical forest plantations are related to leaf traits and tree architecture. *PLoS ONE* 10: e0128084.

Goebes P, Schmidt K, Härdtle W, Seitz S, Stumpf F, von Oheimb G, Scholten T. 2016. Rule-based analysis of throughfall kinetic energy to evaluate biotic and abiotic factor thresholds to mitigate erosive power. *Progress in Physical Geography* 40: 431–449.

Goebes P, Seitz S, Geißler C, Lassu T, Peters P, Seeger M, Nadrowski K, Scholten T. 2014. Momentum or kinetic energy – how do substrate properties influence the calculation of rainfall erosivity? *Journal of Hydrology* 517: 310–316.

Goebes P, Seitz S, Kühn P, Li Y, Niklaus PA, von Oheimb G, Scholten T. 2015b. Throughfall kinetic energy in young subtropical forests: investigation on tree species richness effects and spatial variability. *Agricultural and Forest Meteorology* 213: 148–159.

Gonsamo A, D'odorico P, Pellikka P. 2013. Measuring fractional forest canopy element cover and openness – definitions and methodologies revisited. *Oikos* 122: 1283–1291.

Gunn R, Kinzer GD. 1949. The terminal velocity of fall for water droplets in stagnant air. *Journal of Meteorology* 6: 243–248.

Hall RL, Calder IR. 1993. Drop size modification by forest canopies: measurements using a disdrometer. *Journal of Geophysical Research – Atmospheres* 98: 18465–18470.

Hämmerle M, Lukač N, Chen K-C, Koma Z, Wang C-K, Anders K, Höfle B. 2017. Simulating various terrestrial and UAC LiDAR scanning configurations for understory forest structure modelling. ISPRS *Annals of the* Photogrammetry. *Remote Sensing and Spatial Information Sciences* IV-2(W4): 59–65.

Herwitz SR. 1985. Interception storage capacities of tropical rainforest canopy trees. *Journal of Hydrology* 77: 237–252.

Herwitz SR. 1987. Raindrop impact and water flow on the vegetative surfaces of trees and the effects on stemflow and throughfall generation. *Earth Surface Processes and Landforms* 12: 425–432.

Hiraoka M, Onda Y. 2012. Factors affecting the infiltration capacity in bamboo groves. *Journal of Forest Research* 17: 403–412.

Holder CD. 2012. The relationship between leaf hydrophobicity, water droplet retention, and leaf angle of common species in a semi-arid region of the western United States. *Agricultural and Forest Meteorology* 152: 11–16.

Holder CD. 2013. Effects of leaf hydrophobicity and water droplet retention on canopy storage capacity: leaf hydrophobicity, water droplet retention, and canopy storage capacity. *Ecohydrology* 6: 483–490.

Hollaus M, Wagner W, Molnar G, Mandlburger G, Nothegger C, Otepka J. 2010. Delineation of vegetation and building polygons from full-waveform airborne LiDAR data using Opals Software 7. In *A special joint symposium of ISPRS Technical Commission IV & AutoCarto in conjunction with ASPRS/CaGIS 2010 Fall Specialty Conference*, 15–19 November, Orlando, FL.

Hosoi F, Nakai Y, Omasa K. 2010. Estimation and error analysis of woody canopy leaf area density profiles using 3-D airborne and ground-based scanning Lidar remote-sensing techniques. *IEEE Transactions on Geoscience and Remote Sensing* 48: 2215–2223.

Kattenborn T, Eichel J, Fassnacht FE. 2019a. Convolutional Neural Networks enable efficient, accurate and fine-grained segmentation of plant species and communities from high-resolution UAV imagery. *Science Reports* 9: 17656: 1–9.

Kattenborn T, Lopatin J, Förster M, Braun AC, Fassnacht FE. 2019b. UAV data as alternative to field sampling to map woody invasive species based on combined Sentinel-1 and Sentinel-2 data. *Remote Sensing of Environment* 227: 61–73.

Korpela I, Hovi A, Morsdorf F. 2012. Understory trees in airborne LiDAR data—selective mapping due to transmission losses and echo-triggering mechanisms. *Remote Sensing of Environment* 119: 92–104.

Lacombe G, Valentin C, Sounyafong P, de Rouw A, Soulileuth B, Silvera N, Pierret A, Sengtaheuanghoung O, Ribolzi O. 2018. Linking crop structure, throughfall, soil surface conditions, runoff and soil detachment: 10 land uses analyzed in Northern Laos. *Science of the Total Environment* 616–617: 1330–1338.

Lefsky MA, Cohen WB, Parker GG, Harding DJ. 2002. Lidar remote sensing for ecosystem studies: Lidar, an emerging remote sensing technology that directly measures the three-dimensional distribution of plant canopies, can accurately estimate vegetation structural attributes and should be of particular interest to forest, landscape, and global ecologists. *AIBS Bulletin* 52(1): 19–30.

Levia DF, Germer S. 2015. A review of stemflow generation dynamics and stemflow-environment interactions in forests and shrublands: stemflow review. *Reviews of Geophysics* 53: 673–714.

Levia DF, Herwitz SR. 2000. Physical properties of water in relation to stemflow leachate dynamics: Implications for nutrient cycling. *Canadian Journal of Forest Research* 30: 662–666.

Levia DF, Hudson SA, Llorens P, Nanko K. 2017. Throughfall drop size distributions: a review and prospectus for future research. Wiley Interdisciplinary Reviews: Water e1225.

Levia DF, Michalzik B, Näthe K, Bischoff S, Richter S, Legates DR. 2015. Differential stemflow yield from European beech saplings: the role of individual canopy structure metrics: stemflow and canopy structure. *Hydrological Processes* 29: 43–51.

Levia DF, Nanko K, Amasaki H, Giambelluca TW, Hotta N, Iida S, Mudd RG, Nullet MA, Sakai N, Shinohara Y, Sun X, Suzuki M, Tanaka N, Tantasirin C, Yamada K. 2019. Throughfall partitioning by trees. *Hydrological Processes* 33: 1698–1708.

Liu J, Liu W, Zhu K. 2018. Throughfall kinetic energy and its spatial characteristics under rubber-based agroforestry systems. *Catena* 161: 113–121.

Liu T, Luo J, Zheng Z, Li T, He S. 2016. Effects of rainfall intensity on splash erosion and its spatial distribution under maize canopy. *Natural Hazards* 84(1): 233–247.

Morgan RPC. 2005. *Soil Erosion and Conservation*, third edn. Malden, MA: Blackwell Publishers.

Murakami S. 2006. A proposal for a new forest canopy interception mechanism: splash droplet evaporation. *Journal of Hydrology* 319: 72–82.

© 2020 The Authors. Earth Surface Processes and Landforms published by John Wiley & Sons Ltd

Earth Surf. Process. Landforms, Vol. **45**, 1487–1498 (2020)

Nanko K, Hotta N, Suzuki M. 2006. Evaluating the influence of canopy species and meteorological factors on throughfall drop size distribution. *Journal of Hydrology* **329**: 422–431.

Nanko K, Hudson SA, Levia DF. 2016. Differences in throughfall drop size distributions in the presence and absence of foliage. *Hydrological Sciences Journal* **61**: 620–627.

Nanko K, Mizugaki S, Onda Y. 2008a. Estimation of soil splash detachment rates on the forest floor of an unmanaged Japanese cypress plantation based on field measurements of throughfall drop sizes and velocities. *Catena* **72**: 348–361.

Nanko K, Onda Y, Ito A, Moriwaki H. 2008b. Effect of canopy thickness and canopy saturation on the amount and kinetic energy of throughfall: an experimental approach. *Geophysical Research Letters* **35**: L05401:1–5.

Nanko K, Watanabe A, Hotta N, Suzuki M. 2013. Physical interpretation of the difference in drop size distributions of leaf drips among tree species. *Agricultural and Forest Meteorology* **169**: 74–84.

Panagos P, Ballabio C, Borrelli P, Meusburger K, Klik A, Rousseva S, Tadić MP, Michaelides S, Hrabalíková M, Olsen P, Aalto J, Lakatos M, Rymszewicz A, Dumitrescu A, Beguería S, Alewell C. 2015. Rainfall erosivity in Europe. *Science of the Total Environment* **511**: 801–814.

Panagos P, Meusburger K, Ballabio C, Borrelli P, Alewell C. 2014. Soil erodibility in Europe: a high-resolution dataset based on LUCAS. *Science of the Total Environment* **479–480**: 189–200.

Park A, Cameron JL. 2008. The influence of canopy traits on throughfall and stemflow in five tropical trees growing in a Panamanian plantation. *Forest Ecology and Management* **255**: 1915–1925.

Popescu SC, Wynne RH, Nelso RF. 2002. Estimating plot-level tree heights with lidar: local filtering with a canopy-height based variable window size. *Computers and Electronics in Agriculture* **37**(1–3): 71–95.

Popescu SC, Zhao K. 2008. A voxel-based lidar method for estimating crown base height for deciduous and pine trees. *Remote Sensing of Environment* **112**(3): 767–781.

R Core Team. 2016. *R: A Language and Environment for Statistical Computing*. R Foundation for Statistical Computing: Vienna.

Rosado BHP, Holder CD. 2013. The significance of leaf water repellency in ecohydrological research: a review: leaf water repellency in ecohydrological research. *Ecohydrology* **6**: 150–161.

Roussel JR, Auty D. 2019. lidR: airborne LiDAR data manipulation and visualization for forestry applications. R package version 2.1.4. https://CRAN.R-project.org/package=lidR

Rutter A, Kershaw K, Robins P, Morton A. 1971. A predictive model of rainfall interception in forests, 1. Derivation of the model from observations in a plantation of Corsican pine. *Agricultural Meteorology* **9**: 367–384.

Schmid M, Ehlers TA, Werner C, Hickler T, Fuentes-Espoz JP. 2018. Effect of changing vegetation and precipitation on denudation–Part 2: predicted landscape response to transient climate and vegetation cover over millennial to million-year timescales. *Earth Surface Dynamics* **6**(4): 859–881.

Scholten T, Geißler C, Goc J, Kühn P, Wiegand C. 2011. A new splash cup to measure the kinetic energy of rainfall. *Journal of Plant Nutrition and Soil Science* **174**: 596–601.

Seitz S, Goebes P, Zumstein P, Assmann T, Kühn P, Niklaus PA, Schuldt A, Scholten T. 2015. The influence of leaf litter diversity and soil fauna on initial soil erosion in subtropical forests: influence of leaf litter diversity and soil fauna on soil erosion. *Earth Surface Processes and Landforms* **40**: 1439–1447.

Shinohara Y, Ichinose K, Morimoto M, Kubota T, Nanko K. 2018. Factors influencing the erosivity indices of raindrops in Japanese cypress plantations. *Catena* **171**: 54–61.

Van Dijk A, Bruijnzeel LA. 2001. Modelling rainfall interception by vegetation of variable density using an adapted analytical model. Part 1. Model description. *Journal of Hydrology* **247**: 230–238.

Van Dijk A, Bruijnzeel LA, Rosewell CJ. 2002. Rainfall intensity–kinetic energy relationships: a critical literature appraisal. *Journal of Hydrology* **261**: 1–23.

Wainwright J, Parsons AJ, Abrahams AD. 1999. Rainfall energy under creosotebush. *Journal of Arid Environments* **43**: 111–120.

Wang B, Zheng F, Römkens MJM. 2013. Comparison of soil erodibility factors in USLE, RUSLE2, EPIC and Dg models based on a Chinese soil erodibility database. *Acta Agriculturae Scandinavica Section B Soil and Plant Science* **63**: 69–79.

Wang PK, Pruppacher HR. 1977. Acceleration to terminal velocity of cloud and raindrops. *Journal of Applied Meteorology* **16**(3): 275–280.

Weinacker H, Koch B, Weinacker R. 2004. TREESVIS: a software system for simultaneous ED-real-time visualisation of DTM, DSM, laser raw data, multispectral data, simple tree and building models. *The International Archives of the Photogrammetry, Remote Sensing and Spatial Information Sciences* **36**: 90–95.

Wischmeier WH, Smith DD et al. 1978. Predicting rainfall erosion losses – a guide to conservation planning. In *Predicting Rainfall Erosion Losses: A Guide to Conservation Planning*. US Government Printing Office: Washington, DC.

Wood EM, Pidgeon AM, Radeloff VC, Keuler NS. 2012. Image texture as a remotely sensed measure of vegetation structure. *Remote Sensing of Environment* **121**: 516–526.

Zhongming W, Lees BG, Feng J, Wanning L, Haijing S. 2010. Stratified vegetation cover index: A new way to assess vegetation impact on soil erosion. *Catena* **83**: 87–93.